JOURNAL OF MATERIALS SCIENCE 32 (1997) 4783–4791

The austempering kinetics and mechanical properties of an austempered Cu–Ni–Mo–Mn alloyed ductile iron

M. BAHMANI, R. ELLIOTT
Manchester Materials Science Centre, University of Manchester, Grosvenor Street, Manchester M1 7HS, UK

N. VARAHRAM
Sharif University of Technology, Tehran, Iran

Measurements of austempering kinetics and mechanical properties are presented as a function of austempering time over the range 1–4320 min for different combinations of austempering temperature (275, 315, 370 and 400 °C) and austenitizing temperature (870, 900 and 950 °C) for a ductile iron of composition 3.5% C, 2.6% Si, 0.48% Cu, 0.96% Ni, 0.27% Mo and 0.25% Mn. The austempering kinetics are used to calculate processing windows for the three austenitizing temperatures. The mechanical properties are analysed to show that the processing windows accurately predict the austempering times over which the mechanical properties satisfy the ASTM standard. The analysis shows the role of austenitizing temperature, austempering temperature and time in optimizing the mechanical properties.

1. Introduction

Details have been given elsewhere [1] of the use of an austempered ductile iron of composition 3.5% C, 2.6% Si, 0.5–0.6% Cu, 0.95–1.0% Ni, 0.25–0.30% Mo and 0.25–0.30% Mn to replace steel in two mass produced crankshafts. An important part of this exercise was the selection of the austempering conditions to be used to ensure sufficient hardenability and to satisfy the minimum properties defined for grade 1 in the ASTM A897M:1990 ADI standard. The final selection was made on the basis of processing windows calculated from austempering kinetic measurements. The standard is given in Table I.

The austempering reaction at the high austempering temperatures (370–400 °C) required to produce a high ductility grade of the iron occurs in two stages. In stage I the low C austenite transforms into bainitic ferrite and high C austenite. In stage II the high C austenite transforms into ferrite and carbide. In an iron that is alloyed to achieve hardenability and austempered at high temperatures stage I and stage II reactions can overlap in austempering time. The presence of unreacted low C austenite, in the form of martensite at room temperature, from the stage I reaction and carbide from the stage II reaction is detrimental to the ductility of the austempered iron. Consequently, the selection of the correct austempering treatment (austenitizing temperature, austempering temperature and time) is important.

The processing window defines the austempering time interval, for selected austenitizing and austempering temperatures, over which the amount of these undesirable microstructural phases is not sufficient to prevent the ASTM standard being satisfied. The start of the processing window (time, t_1) has been defined as the austempering time at which the amount of unreacted, low C austenite has been reduced to 3%. The end of the processing window (time, t_2) has been defined as the time at which the maximum retained austenite level has been reduced by 10%. Previous studies [2–5] have shown that processing windows calculated in this way for ductile irons alloyed with Cu–Ni and Mo–Mn–Cu predict successfully the austempering conditions to be used to satisfy the ASTM standard. Processing windows for an iron alloyed with Cu–Ni–Mo–Mn are presented in this paper and mechanical property measurements of austempered irons are used to assess the success of the processing window predictions.

2. Experimental procedure

The ductile iron was produced in the form of keel blocks in an industrial foundry using electric melting. Specimens with dimensions of $15 \times 10 \times 10$ mm were machined from the bottom section of the keel blocks and used to follow the microstructural changes and the changes in retained austenite volume fraction, $X_{\gamma'}$ hardness, austenite C content, $C_{\gamma'}$ and the unreacted austenite volume fraction (UAV) during austempering. Austenitizing was performed under argon for 120 min in an electrically heated furnace. Austempering was performed by rapidly transferring specimens from the austenitizing furnace to a salt bath containing Cassel T.S. 220 (K, $NaNO_3$) salt held at the

0022–2461

TABLE I Grade of the ASTM 897M:1990 ADI standard

Grade	Tensile strength ($N\,mm^{-2}$)	Yield strength ($N\,mm^{-2}$)	Elongation (%)	Impact energy (J)	Typical hardness (BHN)
1	850[a]	550[a]	10[a]	100	269–321
2	1050[a]	700[a]	7[a]	80	302–363
3	1200[a]	850[a]	4[a]	60	341–444
4	1400[a]	1100[a]	1[a]	35	388–477
5	1600[a]	1300[a]	N/A	N/A	444–555

[a] Minimum values.

austempering temperature and isothermally transforming for times in the range 1–4320 min. The specimens were air cooled after austempering.

The changes in C_γ and X_γ were recorded using X-ray diffraction with graphite monochromated CuK_α radiation at 40 kV and 20 mA. A Philips diffractometer with a strip chart recorder was used to scan the angular 2θ range from 40 to 85° three times for each sample. The **C** content was calculated from the angular position of the austenite peaks and the volume fraction of the retained austenite was determined from the integrated area under the austenite and ferrite peaks. At least three measurements were made for each specimen. Details of these calculations have been given elsewhere [2]. UAV measurements were made using a Swift automatic point counter on polished and etched specimens. UAV areas of martensite or untransformed low C austenite could be distinguished easily in the etched microstructure. At least 2000 points were counted using a magnification of $\times 400$. The number of counts was increased with decreasing UAV to maintain a low standard deviation. Hardness measurements were made on a standard Vickers hardness machine with a 10 kg load.

Tensile specimens conforming to ASTM A897M:1990 and unnotched Charpy specimens conforming to ASTM E375 were machined from the bottom section of the keel blocks. After austempering, tensile testing was performed in a 100 kN hydraulic Instron 4500 universal testing machine using a constant cross-beam travel speed of 1 mm min^{-1}. A minimum of two specimens was tested for each heat treatment condition. The ultimate tensile strength (UTS), 0.2% proof strength and elongation to fracture were recorded. The austempered unnotched Charpy specimens were tested at room temperature in a standard Losenhausenwerk impact testing machine. At least two samples were tested for each heat treatment condition.

3. Results and discussion

3.1. Microstructural characteristics of the as-cast iron

The as-cast structure showed a bull's-eye structure with ferrite surrounding the graphite nodules in a pearlitic matrix with a few intercellular carbides. Quantitative analysis showed that there was 79% pearlite, 9.5% ferrite and 11.5% graphite present. The nodule count in the bottom section of the keel block from where specimens were machined was 90–100 mm^{-2} and the nodularity was 78–80%.

3.2. Austempering kinetics

The variation of hardness, retained austenite content, $X_{\gamma'}$ average austenite C content, C_γ and UAV with austempering time can all be used to gain information concerning the kinetics of the stage I and stage II reactions in the austempering process. The progress of the stage I reaction is accompanied by an increase in X_γ and C_γ, and by a decrease in hardness and UAV. The stage II reaction produces an increase in hardness and a decrease in X_γ. The change in these parameters with austempering time for different combinations of austempering (400, 370, 315 and 275 °C) and austenitizing (870, 900 and 950 °C) temperatures is shown in Figs 1–4.

3.2.1. The stage I reaction

In previous studies [2–5] hardness measurements have been used to determine average stage I kinetics. The time, t_H, for the hardness to fall to 100 units above the minimum level has been shown to represent the time for 60–80% of the stage I reaction to be completed. These times are shown in Fig. 5 for the present iron and previous irons containing different alloying additions. The present results show the strong influence of austenitizing temperature on the stage I kinetics. Comparing curves 1, 2 and 3 for the present iron for an austempering temperature of 370 °C shows that reducing the austenitizing temperature from 950 to 870 °C reduces t_H from 18 to 6.5 min. Comparing the present with previous measurements shows the relative influence of different alloying additions on the kinetics. Considering curves 4 and 5 for an austenitizing temperature of 900 °C and an austempering temperature of 370 °C shows that increasing the combined Cu and Ni content by 1.57% produces an increase in t_H from 3 to 5.5 min. On the other hand considering curves 2 and 4 for the same conditions shows that an increase in the combined Mo and Mn contents of 0.52% and a decrease in the combined Cu and Ni contents of 0.46% produces a significant increase in t_H from 5.5 to 12 min. This shows that the delaying effect of Mn and Mo on the stage I reaction is much greater than that of Cu and Ni. This is illustrated again by curves 3 and 6 for an austenitizing temperature of 870 °C and an austempering temperature of

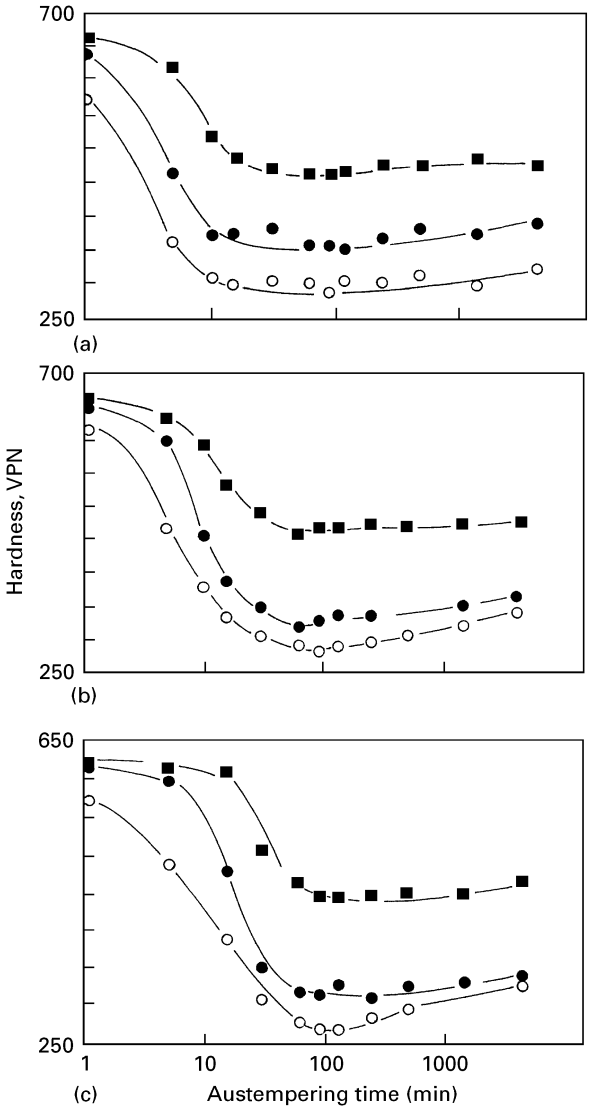

Figure 1 The variation of hardness with austempering time for austempering temperatures of (■) 275, (●) 370 and (○) 400 °C and austenitizing temperatures of (a) 870, (b) 900 and (c) 950 °C.

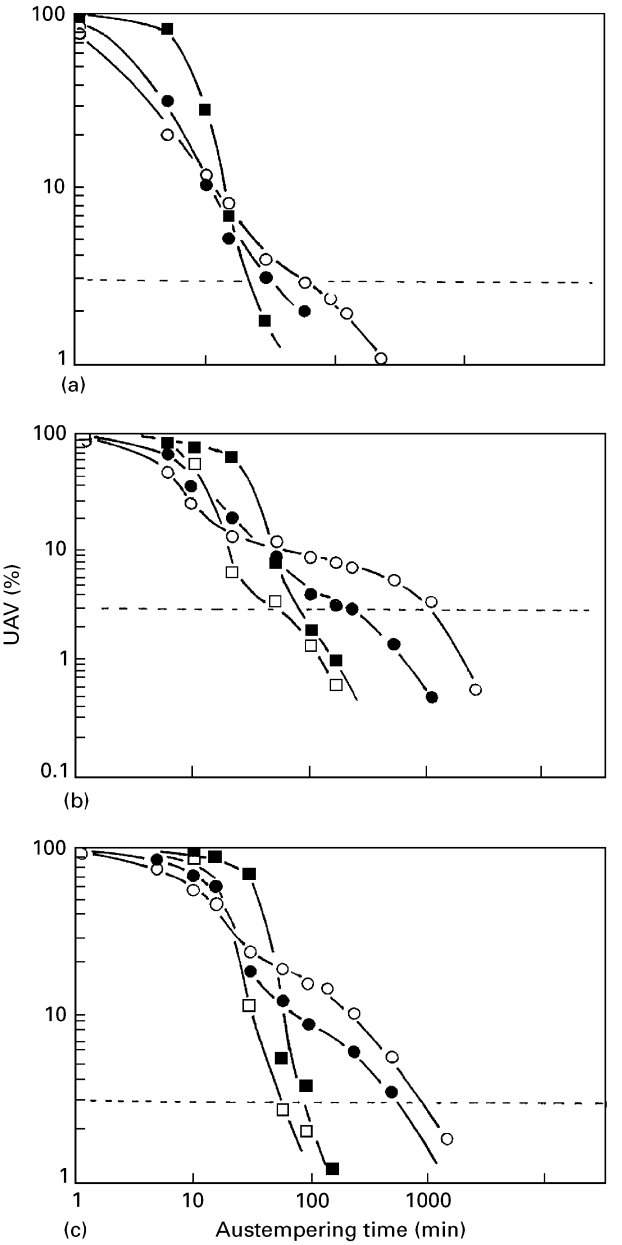

Figure 2 The variation of UAV with austempering temperatures of (■) 275, (□) 315, (●) 370 and (○) 400 °C and austenitizing temperatures of (a) 870, (b) 900 and (c) 950 °C.

370 °C. Under these conditions a decrease of 0.1% in the combined Mo and Mn contents and an increase of 1.15% in the combined Cu and Ni contents produce only a slight increase in t_H. These comparisons illustrate the care that must be exercised in selecting the amount of Mo and Mn present in the iron if delay in the completion of the stage I reaction is to be avoided and how reducing the austenitizing temperature can be used to counteract this effect.

The end of the stage I reaction is of greater significance in selecting the optimum austempering heat treatment cycle. If sufficient unreacted, low C austenite (in the form of martensite) remains in the structure to form continuous paths, the ductility is reduced. Previous studies [2–5] have shown that this critical level of UAV is about 3%. A hardness indentation covers several eutectic cells. Consequently, a hardness measurement is an average value and is not particularly sensitive to the changes that occur in the small volume of intercellular boundaries late in the stage I reaction. These changes can be observed directly using optical microscopy. Double etching [6] of the sample allows a clear distinction to be made between unreacted and reacted (high C austenite) areas. Point counting can be used to measure the UAV accurately. These measurements are shown in Fig. 2. The microstructural observations show that the stage I reaction starts close to the graphite nodules, progresses through the eutectic cell and then, at a time that is influenced strongly by the austempering conditions, occurs in the intercellular boundary areas. The later start in the intercellular areas is due to the delaying effect of Mn and Mo and due to the segregation of Mn and Mo to the intercellular areas. These effects are clearly evident in Fig. 6, which shows the UAV measurements for an austempering temperature of 400 °C and austenitizing temperatures of 870 and 900 °C. Curves A and C show that the UAV does not fall continuously, as occurs in an iron without alloying additions, but shows an arrest that is due to the delayed stage I reaction in the intercellular areas. Curve A can be divided into curves B and D to represent the changes in the eutectic cell

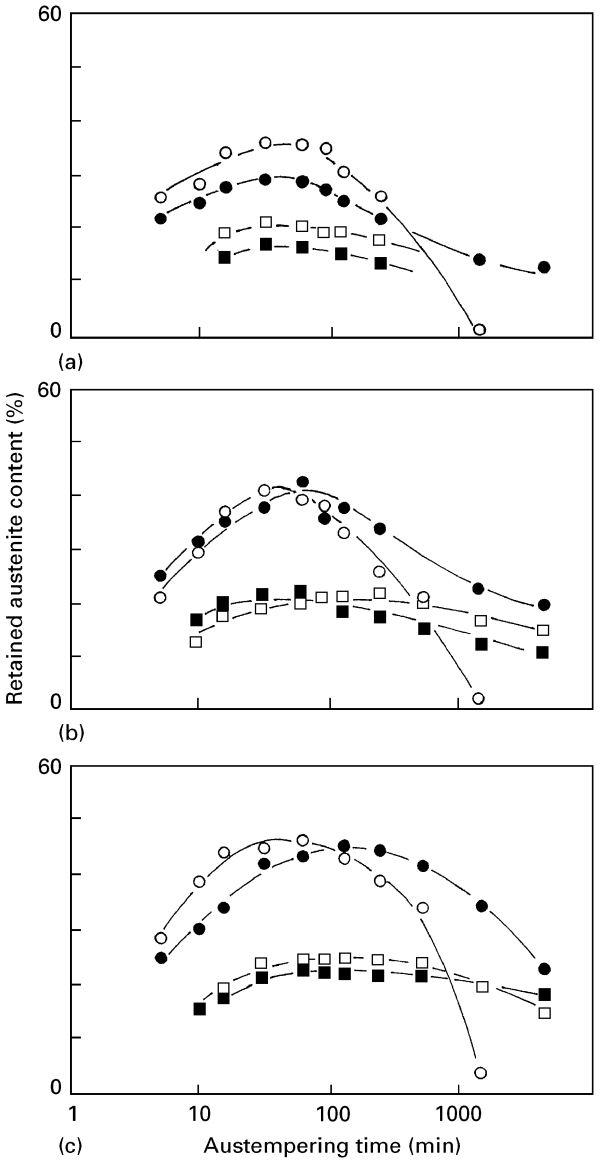

Figure 3 The variation of retained austenite content with austempering time for austempering temperatures of (■) 275, (□) 315, (●) 370 and (○) 400 °C and austenitizing temperatures of (a) 870, (b) 900 and (c) 950 °C.

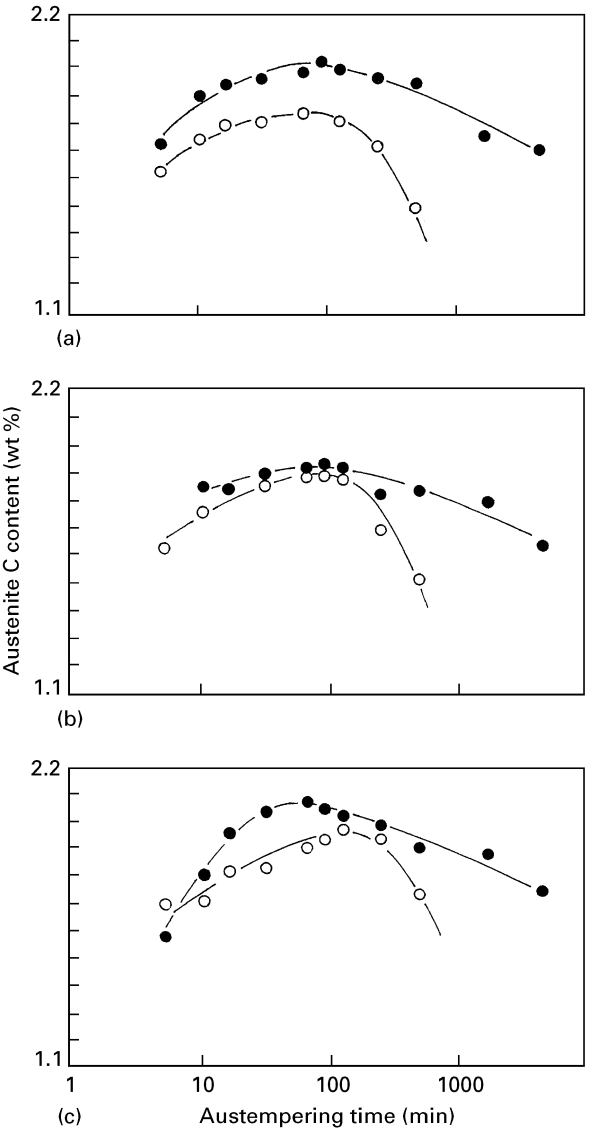

Figure 4 The variation of austenite C content with austempering time for austempering temperatures of (●) 370 and (○) 400 °C and austenitizing temperatures of (a) 870, (b) 900 and (c) 950 °C.

and intercellular areas, respectively. Curve B suggests that the stage I reaction begins in the eutectic cell after a few minutes and occurs continuously until completion (UAV = 1%) after about 50 min. On the other hand, curve D suggests that the stage I reaction does not start in the segregated intercellular area until after 40 min and is not completed until after 1000 min. The critical 3% level is not achieved until after 500 min, a time well in excess of that used normally for austempering. Curve C for the lower austenitizing temperature shows the same general features as curve A, but the stage I reaction occurs at an earlier time in all areas of the structure and the critical 3% level is achieved in the intercellular area at a much earlier time of about 60 min. These events are confirmed from the microstructural observations. The times recorded for the completion of 60–80% of the stage I reaction from the hardness measurements are shown as filled squares on curves A and C. It is interesting to note that both points lie between the 60–80% completion levels determined from the UAV measurements. Finally, values of the time t_1, can be measured from the results recorded in Fig. 2.

3.2.2. The stage II reaction

The carbide formed in the stage II reaction is detrimental to the mechanical properties. Unfortunately, it is extremely fine and cannot be observed under the optical microscope. Several transmission electron microscope (TEM) studies [7–10] have been reported recently identifying carbides formed in irons of different compositions. At present these studies are not sufficiently extensive to give a complete picture of the stage II reaction. It has been suggested [10] that carbide formation at ferrite–austenite phase boundaries restricts the plastic zone ahead of a crack allowing easy crack propagation along the interface resulting in reduced ductility. At present the most informative method of following the stage II reaction kinetics is to use the fall in X_γ recorded in Fig. 3. This data can be normalized using $X_{\gamma'}^{\max}$ the maximum

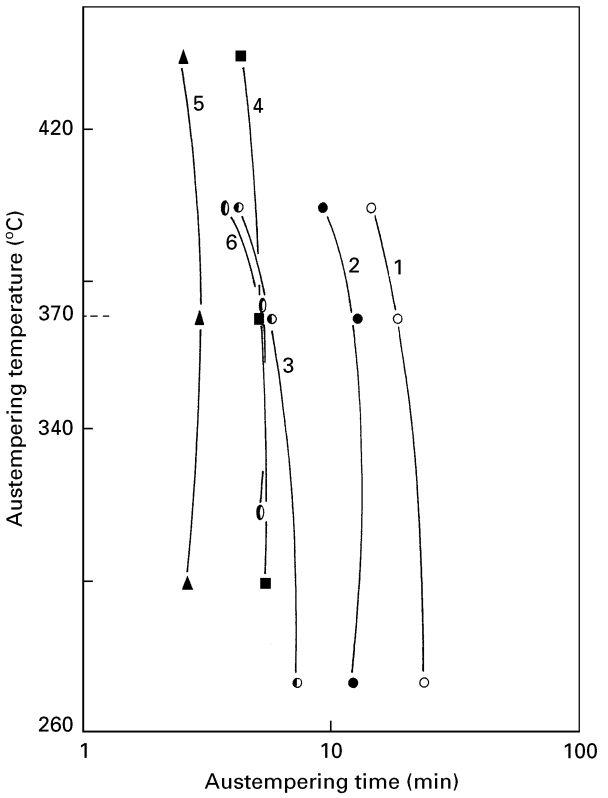

Figure 5 The variation of time to reach a hardness 100 units above the minimum with austempering temperature for irons of different composition. Curves 1–3, this study; curves 4 and 5 from [2]; curve 6 from [5]. Austempering temperatures: (◐) 870 °C [5], (◐) 870 °C, this study; (▲) 900 °C [2], (■) 900 °C [2], (●) 900 °C, this study; (○) 950 °C, this study.

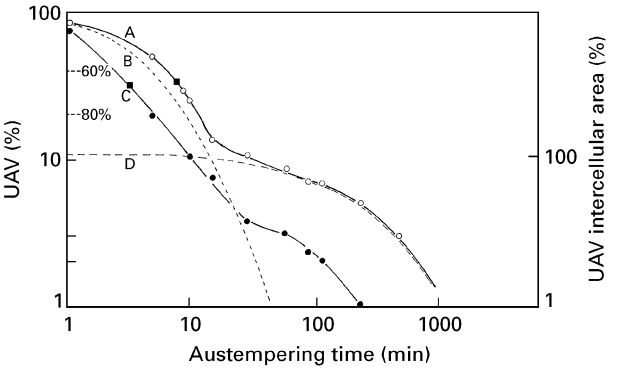

Figure 6 The variation of UAV with austempering time divided to show the different stage I reactions in the eutectic cell and intercellular region. Austempering temperature, 400 °C. Curves A and C show the overall changes at austenitizing temperatures of 900 and 870 °C, respectively. Curves B and D give the traces of the eutectic cell and the intercellular region at an austenitizing temperature of 900 °C.

retained austenite content. The ratio X_γ/X_γ^{max} falls from 1 to 0 as the stage II reaction proceeds. Normalized data are shown in Fig. 7 for different austempering and austenitizing temperatures. These results show that the stage II reaction is controlled mainly by the austempering temperature. In contrast to the stage I reaction the austenitizing temperature does not have as strong an influence. Finally, values for the time t_2, defined as the time at which the maximum high C aus-

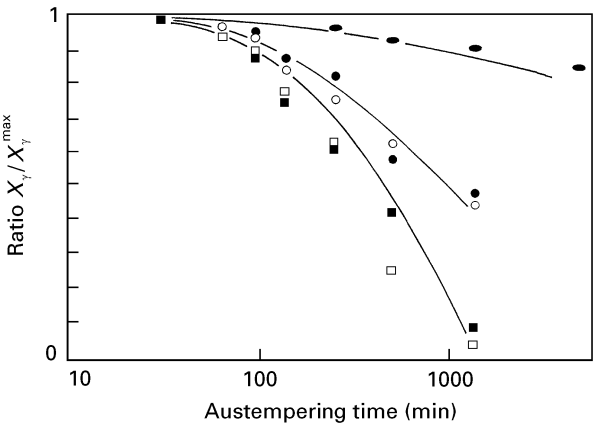

Figure 7 The variation of the ratio X_γ/X_γ^{max} with austempering time for austempering temperatures of 315, 370 and 400 °C and austenitizing temperatures of 870, 900 and 950 °C: (■) 400, 900 °C; (□) 400, 870 °C; (●) 370, 900 °C; (○) 370, 870 °C; (⬬) 315, 900 °C.

tenite content has been reduced by 10% and the end of the processing window, are determined from Fig. 3.

3.2.3. The processing window

The processing window defines austempering times within which optimum mechanical properties, particularly ductility, that satisfy the ASTM A897:1990 standard are achieved in the austempered iron. The values of t_1 and t_2 determined from the austempering kinetic measurements and the corresponding processing windows for austenitizing temperatures of 870, 900 and 950 °C are shown in Fig. 8. In common with windows defined for irons of different compositions Fig. 8 shows:

1. At each austenitizing temperature the processing window is relatively wide at austempering temperatures in the lower bainite range used to produce high strength grades of the standard.
2. At higher austempering temperatures used to produce the more ductile grades of the standard the window narrows and eventually closes.
3. Decreasing the austenitizing temperature has two effects on the processing window: (i) it increases the closure temperature (Fig. 8 predicts a closure temperature of 415, 375 and 360 °C for austenitizing temperatures of 870, 900 and 950 °C, respectively); and (ii) the processing window is moved to earlier austempering times.

Fig. 8 suggests that difficulty might be experienced in satisfying the ASTM standard for high ductility grades and careful selection of the austenitizing temperature, austempering temperature and time are required.

3.3. Mechanical properties of the austempered iron

As the present iron is to be used in the mass production of crankshafts requiring the high ductility grade 1 or grade 2 of the ASTM standard, mechanical property measurements were concentrated on irons

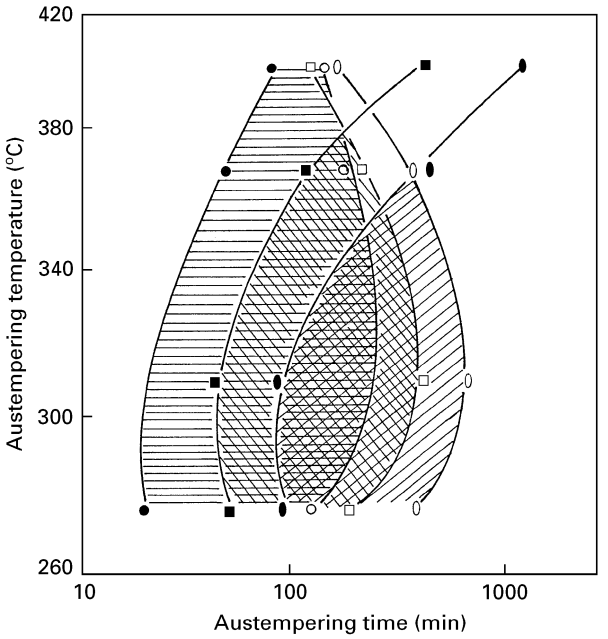

Figure 8 Processing windows for austenitizing temperatures of (▤) 870, (▧) 900 and (▨) 950 °C. The time t_1 is that at which the unreacted austenite content has fallen to 3%. The time t_2 is that at which the retained austenite content has fallen to 90% of its maximum value. t_1: (●) 870, (■) 900, (⬮) 950 °C. t_2: (○) 870, (□) 900, (⬭) 950 °C.

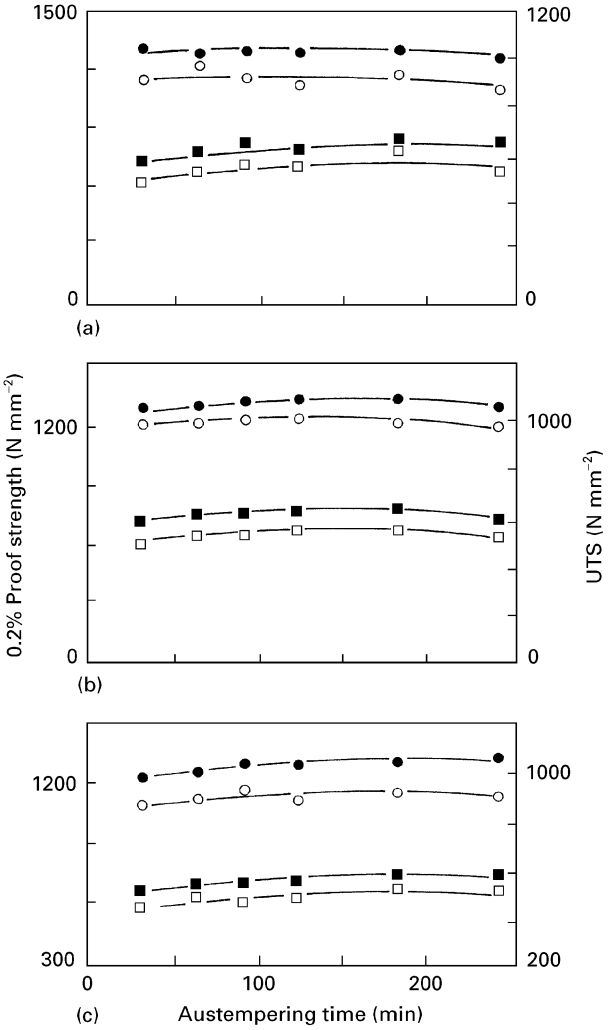

Figure 9 The variation of (●, ○) UTS and (■, □) 0.2% proof strength with austempering time for austempering temperatures of (●, ■) 370 and (○, □) 400 °C and austenitizing temperatures of (a) 870, (b) 900 and (c) 950 °C.

austempered at 370 and 400 °C and for times likely to be used in commercial production (up to 4 h). Measurements of the UTS and 0.2% proof strength are shown in Fig. 9. Measurements of elongation and unnotched Charpy energy are shown in Fig. 10. The three parameters austenitizing temperature, austempering temperature and time, control the austempering kinetics (as described in Section 3.2), the microstructure and the mechanical properties. Their influence on mechanical properties is described below.

3.3.1. Influence of austempering temperature

The choice of austempering temperature determines the grade of alloyed ductile ion produced primarily through its influence on strength. Fig. 11 shows the variation in mechanical properties with austempering temperature for an austempering time of 120 min. This time was selected because it is a commonly used austempering time and for the present composition is close to the time producing optimum properties. However, there will be a small dependence on austempering time because of the influence of austenitizing temperature on the kinetics. Fig. 11 shows that a low austempering temperature promotes strength. Structural features responsible for this are a fine dispersion of ferrite platelets, dispersed carbide and a low level of austenite. The needle-like morphology of the ferrite, carbides and the low level of austenite contribute to the low ductility. The highest ductility at low austempering temperature occurs at the highest austenitizing temperature. This is due to the higher C content stabilizing the austenite. At the highest austempering temperature the driving force for the stage I reaction is lower and that for the stage II reaction is higher. As a result the austempered microstructure is less uniform and can contain blocky austenite regions with martensite in their centre. In addition, the stage I and stage II reactions can overlap. The result of these effects is that the strength continues to fall slowly while the ductility decreases more rapidly.

Fig. 11 shows that a strength of 1350 N mm^{-2} with elongations of about 4% can be achieved with an austempering temperature of 315 °C, which satisfies grade 3 of the ASTM standard. Strengths approaching 1000 N mm^{-2} and elongations approaching 12% can be achieved with an austempering temperature of 370 °C. These properties satisfy grade 1 of the standard.

3.3.2. The influence of austempering time

Once the austempering temperature has been selected, austempering time is chosen to optimize the mechanical properties. The variation of UTS and 0.2% proof strength with austempering time for austempering temperatures of 370 and 400 °C is shown in Fig. 9 and that for elongation and unnotched Charpy energy in Fig. 10. The variation of mechanical properties with austempering time depends on the change in the

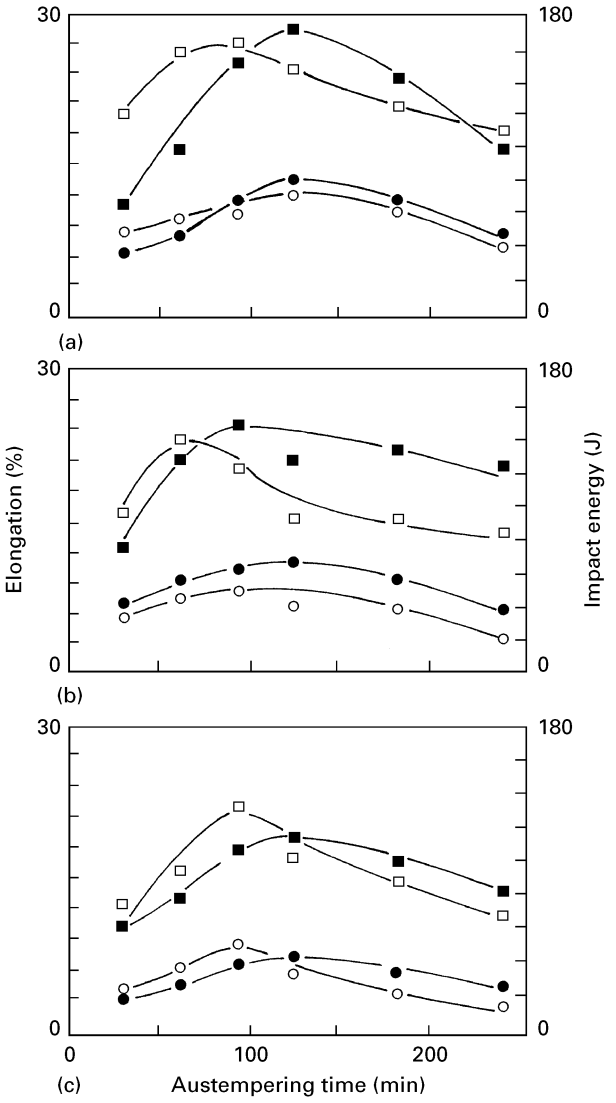

Figure 10 The variation of (●, ○) elongation and (■, □) impact energy with austempering time for austempering temperatures of (●, ■) 370 and (○, □) 400 °C and austenitizing temperatures of (a) 870, (b) 900 and (c) 950 °C.

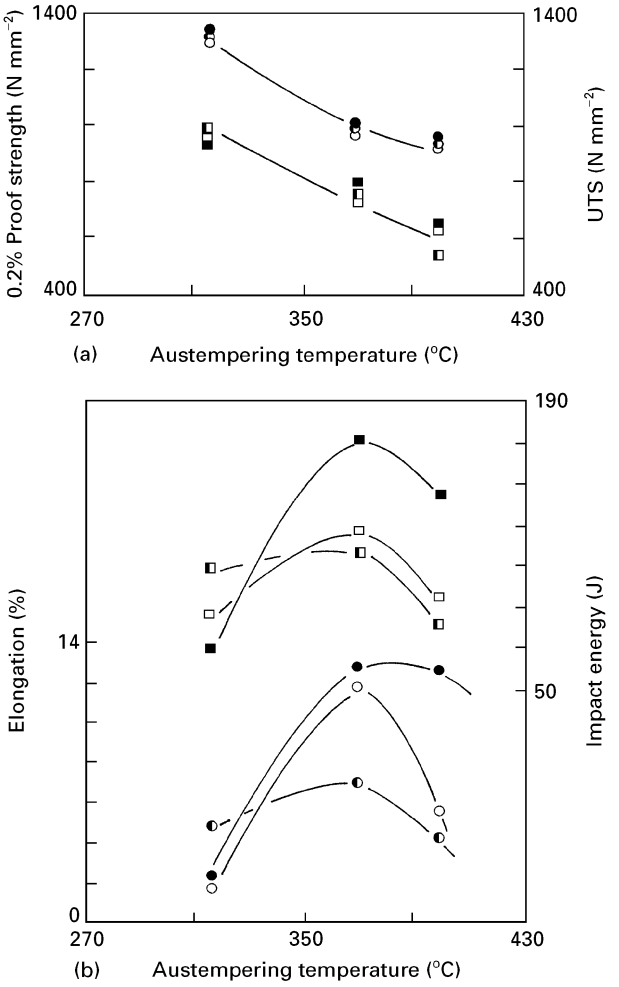

Figure 11 The variation of (a) UTS (square symbols) and 0.2% proof strength (circular symbols); and (b) elongation (circular symbols) and impact energy (square symbols) with austempering temperature for austenitizing temperatures of (●, ■) 870, (○, □) 900 and (◐, ◧) 950 °C.

nature and amount of phases present as the austempered structure evolves. With reference to curve A in Fig. 6, as the austempering time increases up to 30 min, the amount of martensite derived from unreacted austenite decreases and the strength, elongation and impact energy increase. After 30 min the stage I reaction in the eutectic cell is nearly completed. As the time increases above 30 min the stage I reaction commences in the intercellular region and the strength and ductility increase further to a maximum that coincides with a tolerable amount of martensite in the intercellular region. Fig. 7 shows that the stage II reaction has commenced after about 60 min and from 100 min the high C austenite level has fallen sufficiently to reduce the ductility. The decrease in strength is much smaller.

3.3.3. The influence of austenitizing temperature

Decreasing the austenitizing temperature reduces the austenite carbon content after austenitizing and increases the driving force for the stage I reduction without having a significant effect on the stage II reaction. This moves the completion of the stage I reaction to earlier austempering times and may alter the time sequence of the microstructural changes in the austempering process. In particular, it may reduce or eliminate any overlap of the stage I and stage II reactions at higher austempering temperatures. This may make it possible to produce a fully ausferrite structure leading to improved mechanical properties. There is evidence for this in Fig. 12, which shows the optimum mechanical properties as a function of austenitizing temperature for austempering temperatures of 315, 370 and 400 °C. Both elongation and impact energy increase sharply with decreasing austenitizing temperature as the processing window is opened. This effect would not be expected to be as significant with lower austempering temperatures as the stage I and stage II reactions do not overlap to the same extent. This is reflected in the smaller change observed for an austempering temperature of 315 °C. The change in strength is not as great as that for elongation and impact energy. The above changes are effective for austenitizing temperatures between 850 and 950 °C. Changes occur below 850 °C due to the introduction

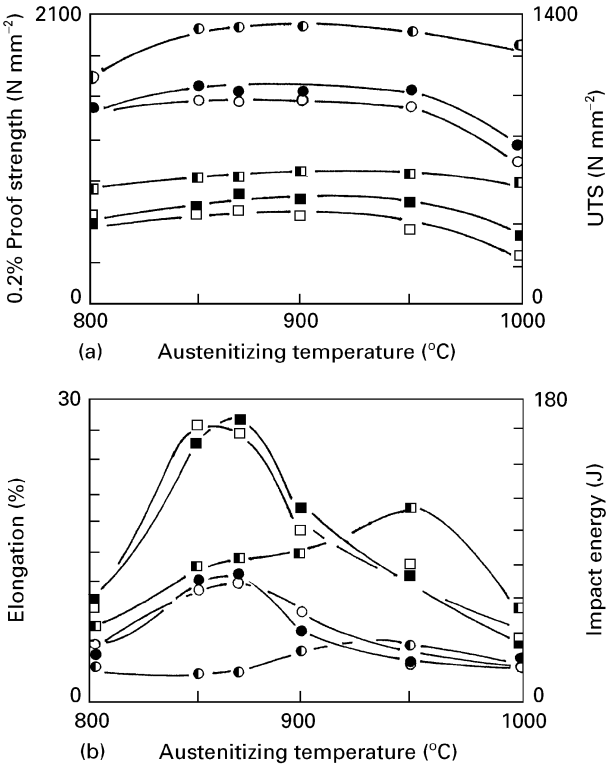

Figure 12 The variation of (a) UTS (square symbols) and 0.2% proof strength (circular symbols); and (b) elongation (circular symbols) and impact energy (square symbols) with austenitizing temperature for austempering temperatures of (◐, ◧) 315, (●, ■) 370 and (○, □) 400 °C.

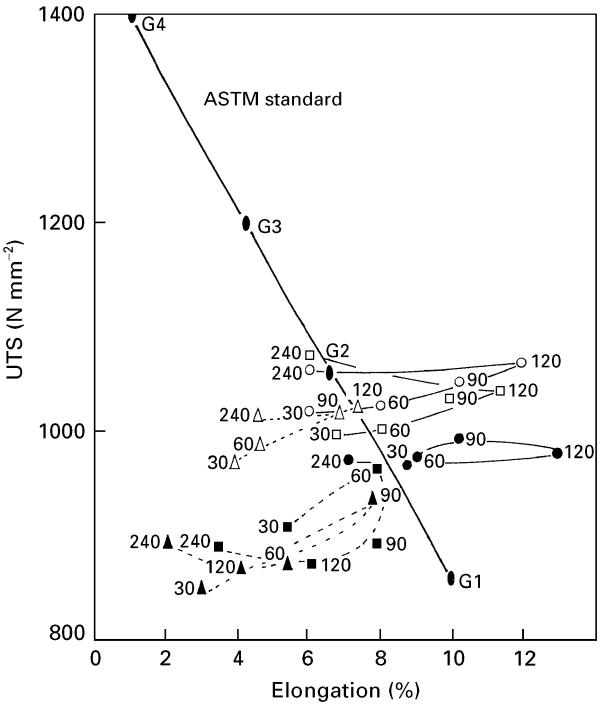

Figure 13 The variation of UTS with elongation for different austempering conditions. The numbers by the points are the austempering times in minutes. Austempering temperature/austenitizing temperature: (○) 370, 870; (□) 370, 900; (△) 370, 950; (●) 400, 870; (■) 400, 900; (▲) 400, 950 °C.

of ferrite into the austenitized structure and above 950 °C due to austenite grain growth and increased overlap of the stage I and stage II reactions that decrease the mechanical properties.

These observations show that the choice of austenitizing temperature is significant in the selection of austempering conditions to achieve high ductility grades. The same benefits are not obtained when using a low austempering temperature. Indeed, Fig. 12 suggests that a higher austenitizing temperature optimizes the mechanical properties.

3.4. Comparison of mechanical properties with the ASTM standard

Fig. 13 shows the tensile properties plotted in the form of a UTS–elongation relationship. Fig. 14 shows the impact properties in the form of a UTS–impact energy relationship. The numbers by the points denote the austempering times. The minimum properties defined for the various grades of the standard are shown in the figures. For the purpose of the present comparison the mechanical properties of the iron are considered to satisfy the standard if the mechanical properties are represented on Figs 13 and 14 by a point that lies above the line joining the points representing the different grades of the standard. In general, the grade of the standard satisfied will be that either to the immediately left or right of the position where the mechanical properties cross the line defining the standard.

Considering Fig. 13 and an austempering temperature of 400 °C, it can be seen that the standard is satisfied only for an austenitizing temperature of 870 °C with the optimum properties achieved with an austempering time of 90–120 min. This shows good agreement with the processing window calculated from the austempering kinetics measurements. Fig. 8 predicts that the window is open only for the 870 °C austenitizing temperature centred on 120 min. Fig. 13 shows that for an austempering temperature of 370 °C the standard is satisfied for austenitizing temperatures of 870 and 900 °C but not for 950 °C. The results in Fig. 8 show that the processing window is open at 870 and 900 °C, but not at 950 °C. The results in Fig. 14 show a similar pattern of behaviour for the impact energy. It has been found in previous studies with alloyed irons that the behaviour of impact energy is similar to that of tensile elongation but the standard is achieved more easily. This pattern of behaviour is evident in the present observations.

The selection of treatments 900 °C–120 min/370 °C–120 min, 870 °C–120 min/370 °C–120 min and 870 °C–120 min/400 °C–120 min will all satisfy grade 1 of the standard in samples that are through hardened during austempering. The trends of property changes in Figs 13 and 14 show that if the requirement is to satisfy grade 2 of the standard, a slightly lower austempering temperature should be used.

4. Conclusions

Measurements of the austempering kinetics of the through hardened, austempered iron are presented

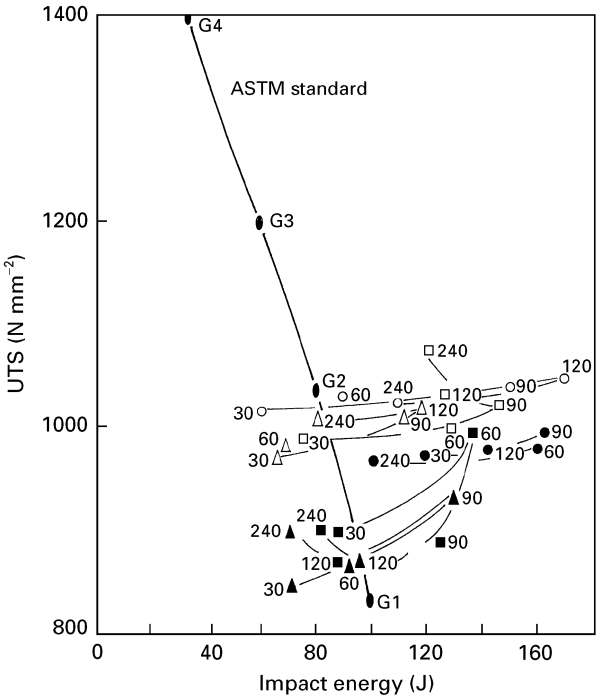

Figure 14 The variation of UTS with unnotched impact energy for different austempering conditions. The numbers by the points are the austempering times in minutes. For a 370 °C austempering temperature: (○) 870, (□) 900, (△) 950 °C austenitizing temperatures. For a 400 °C austempering temperature: (●) 870, (■) 900, (▲) 950 °C austenitizing temperatures.

and used to define processing windows for austenitizing temperatures of 870, 900 and 950 °C. Mechanical property measurements are recorded for different austempering conditions and show that the ASTM standard is satisfied for austempering times defined by the processing windows. The influence of austenitizing temperature, austempering temperature and time on the austempered structure and the mechanical properties is defined.

Acknowledgements

M. B. would like to thank the Iranian Government for financial support. The authors would like to thank Professor G. W. Lorimer for providing laboratory facilities.

References

1. M. BAHMANI, R. ELLIOTT and N. VARAHRAM, *Int. Cast Met. Res. J.* **9** (1997) 249.
2. N. DARWISH and R. ELLIOTT, *Mater. Sci. Technol.* **9** (1993) 882.
3. H. BAYATI and R. ELLIOTT, *ibid.* **11** (1995) 284.
4. A. S. HAMID ALI and R. ELLIOTT, *ibid.* **12** (1996) 679.
5. A. NAZARBOLAND and R. ELLIOTT, *Int. Cast Met. Res. J.* **9** (1997) 295.
6. H. BAYATI, PhD thesis, University of Manchester, Manchester (1996).
7. Y. C. LIU, J. M. SCHISSLER, J. P. CHOBAUT and H. VETTERS, *Metall. Sci. Technol.* **13** (1995) 12.
8. I. GUTIERREZ, J. ARANZABAL, F. CASTRO and J. J. URCOLA, *Met. Trans.* **26A** (1995) 1045.
9. L. SIDJANIN, R. E. SMALLMAN and J. M. YOUNG, *Acta Metall. Mater.* **42** (1994) 3149.
10. Z. K. FAN and R. E. SMALLMAN, *Scripta Metall. Mater.* **31** (1994) 137.

Received 7 August 1996
and accepted 26 February 1997